

Mixture of Scale Experts for Alignment-free RGBT Video Object Detection and A Unified Benchmark

Qishun Wang, Zhengzheng Tu, Kunpeng Wang, Le Gu, Chuanwang Guo

Abstract—Existing RGB-Thermal Video Object Detection (RGBT VOD) methods predominantly rely on the manual alignment of image pairs, that is both labor-intensive and time-consuming. This dependency significantly restricts the scalability and practical applicability of these methods in real-world scenarios. To address this critical limitation, we propose a novel framework termed the Mixture of Scale Experts Network (MSENet). MSENet integrates multiple experts trained at different perceptual scales, enabling the capture of scale discrepancies between RGB and thermal image pairs without the need for explicit alignment. Specifically, to address the issue of unaligned scales, MSENet introduces a set of experts designed to perceive the correlation between RGBT image pairs across various scales. These experts are capable of identifying and quantifying the scale differences inherent in the image pairs. Subsequently, a dynamic routing mechanism is incorporated to assign adaptive weights to each expert, allowing the network to dynamically select the most appropriate experts based on the specific characteristics of the input data. Furthermore, to address the issue of weakly unaligned positions, we integrate deformable convolution into the network. Deformable convolution is employed to learn position displacements between the RGB and thermal modalities, thereby mitigating the impact of spatial misalignment. To provide a comprehensive evaluation platform for alignment-free RGBT VOD, we introduce a new benchmark dataset. This dataset includes eleven common object categories, with a total of 60,988 images and 271,835 object instances. The dataset encompasses a wide range of scenes from both daily life and natural environments, ensuring high content diversity and complexity. Extensive experiments conducted on this benchmark dataset demonstrate the superior performance of our proposed detector compared to other state-of-the-art methods. The results highlight the effectiveness of MSENet in addressing the challenges associated with alignment-free RGBT VOD. To further promote research and development in this domain, we will publicly release our code and the benchmark dataset.

I. INTRODUCTION

THE emergence of RGBT VOD [1] represents a significant advancement over traditional RGB-based VOD systems by incorporating thermal images, which enhances detection robustness, particularly in challenging lighting conditions. Current RGBT VOD methodologies typically depend on aligned RGBT image pairs for training. However, the spatial distribution and scale of objects captured by RGB and thermal sensors differ due to variations in wavelength and focal length [2]. As illustrated in Fig. 1, the objects in the two modalities are completely misaligned, exhibiting substantial scale variations. Even after manual adjustments to correct the object’s scale, weak alignment in the RGBT image pairs persists. As a result, the manual alignment of RGBT data proves to be both challenging and time-consuming, which

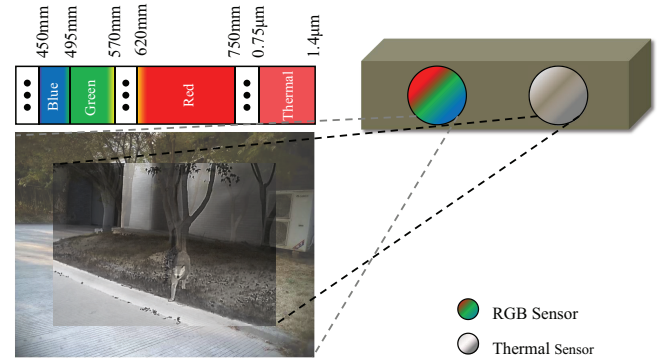


Fig. 1. Multispectral sensors capture images across different wavelengths, leading to significant differences in the scale and field of view of objects. These discrepancies stem from the distinct optical properties and sensor characteristics associated with each wavelength band, resulting in variations in spatial resolution and coverage area.

limits the practical application of RGBT VOD in real-world scenarios.

Currently, most RGBT vision tasks still use aligned image pairs to train multimodal networks. To address this limitation, some researchers have begun to explore how to operate on multimodal image pairs without strict alignment. Zhang *et al.* [3] introduce the Aligned Region CNN (AR-CNN), which employs a region feature alignment module to learn positional offsets and dynamically align multimodal features corresponding to these positions within an end-to-end training framework. To handle multimodal images with significant misalignment, the method proposed by [4] integrates the Intersection over Union (IoU) of both modalities and utilizes a detection head for simultaneous bounding box regression across these modalities. Yuan *et al.* [5] propose a Translation-Scale-Rotation Alignment (TSRA) module designed to align region proposal features from the two modalities. However, this approach is limited to two-stage detectors. Moreover, the weakly aligned image pairs considered by the aforementioned methods are manually aligned to a similar appearance and do not faithfully represent the actual scene, as depicted in Fig. 1.

Recently, some studies have begun to investigate on how to use unaligned RGBT images. Song *et al.* [6] introduce a cross-modal alignment detector that focuses on learning a transformation matrix to align an RGB image with a thermal image. Similarly, Liu *et al.* [7] propose to estimate a homography matrix to achieve the alignment from a thermal image to an RGB image. However, there is a key challenge that semantic differences across modalities influence the reliability of the

estimated transformation matrix potentially.

To address these challenges, we propose a Mixture of Scale Experts (MSE) module, designed to effectively handle the scale discrepancies and misalignments inherent in RGBT image pairs. Specifically, we configure a set of expert sub-modules, each equipped with a distinct scale perception range to capture the varying spatial characteristics of objects across modalities. These expert modules leverage the perceived differences to identify and extract the corresponding regions from the high-resolution RGB image that align with the spatial distribution of the Thermal image, thereby facilitating scale alignment. To further address pixel-level deviations between object positions in the two modalities, we employ deformable convolution. This technique dynamically adjusts sampling positions and learns positional offsets, enabling the network to adaptively correct for misalignments at the pixel level. This is particularly crucial for handling weakly aligned RGBT image pairs, where objects may exhibit significant positional discrepancies. Moreover, each expert module incorporates a scoring branch that evaluates the relevance and contribution of the expert's output to the current input. These scores are subsequently utilized as adaptive weights to dynamically fuse the results from all expert modules. This weighted fusion strategy allows the MSE to effectively adapt to RGBT image pairs with varying scale differences across diverse scenarios, thereby enhancing the robustness and accuracy of the overall system.

On the other hand, the only existing evaluation benchmark for RGBT VOD is the VT-VOD50 dataset [1], which comprises seven categories focused on traffic scenes and consists of 18,898 images. However, VT-VOD50 does not contain the original data but instead offers RGBT image pairs that have been manually cropped, scaled, and aligned. This deviation from the original imaging conditions limits its comprehensiveness for evaluating model performance. In response to this limitation, we propose a more realistic and extensive evaluation benchmark, named UVT-VOD2024, specifically designed for alignment-free RGBT VOD. UVT-VOD2024 encompasses a wider variety of scenes, including rural areas, towns, parks, campuses, and residential neighborhoods. With a total of 11 categories, the dataset includes 60,000 images and 271,000 object instances. In contrast to VT-VOD50, UVT-VOD2024 offers greater temporal series and scene diversity, incorporating various lighting conditions, camera motion displacements, and background complexities. Notably, it retains alignment-free RGBT image pairs derived directly from RGBT sensors. This authentic data allows for a comprehensive evaluation of RGBT VOD methods and provides insights into their potential applicability in real-world scenarios.

In summary, we have designed a Mixture of Scale Experts Network (MSENet) tailored for the alignment-free RGBT VOD task and established a comprehensive evaluation benchmark dataset, UVT-VOD2024. To the best of our knowledge, this represents the pioneering effort to explore the alignment-free RGBT VOD task. Currently, no dedicated benchmark platform exists for evaluating this specific task. The primary contributions of this study are outlined below:

- We design a Mixture of Scale Experts Network (MSENet)

for alignment-free RGBT VOD. Specifically, MSENet utilizes multiple experts that can dynamically perceive and eliminate scale variations across different scenes and further mitigate the misalignment of objects at the instance level through deformable convolution.

- We contribute a benchmark dataset for alignment-free RGBT VOD, comprising 60988 images collected from a variety of real-world scenes. The dataset is used to conduct a comprehensive evaluation and analysis of existing state-of-the-art (SOTA) detectors. It will be made publicly available.
- We assess the performance of our MSENet on the dataset presented within this study, confirming the efficacy of our design and attaining new SOTA results. This study provides a potentially more practical research direction for RGBT VOD.

II. RELATED WORK

A. Video Object Detection

RGB-based VOD aims to effectively utilize temporal multi-frame information. Deng *et al.* [8] propose employing Relation Distillation Networks (RDN) to capture long-range dependencies among objects in videos, thereby improving detection performance. Inspired by the human visual system's ability to observe dynamics in videos, MEGA [9] integrates global and local information comprehensively, leading to improvements in memory utility and achieving state-of-the-art performance at the time. He *et al.* [10] explore the potential of DETR in the VOD field through the design of a Temporal Query Encoder (TQE) and a corresponding decoder. Additionally, Sun *et al.* [11] propose a departure from the conventional two-stage paradigm in traditional VOD by utilizing temporal consistency to filter background areas, thus facilitating efficient single-stage VOD. Similarly, Shi *et al.* [12] choose to model VOD as a single-stage detection problem and perform multi-frame aggregation in the later stages of the network to reduce ineffective low-quality fusion. Sun *et al.* [13] argue that the prior memory structure was excessively redundant. The Hybrid Multi-Attention Transformer (HyMAT) module [14] is proposed to mitigate erroneous feature enhancement arising from positional uncertainty. This design can be seamlessly integrated into either self-attention or cross-attention mechanisms. Therefore, they introduce a multi-level aggregation structure utilizing a memory bank, leading to a significant reduction in computing costs.

Despite advancements, RGB-based VOD continues to face imaging constraints in challenging environments. Tu *et al.* [1] have recently introduced RGBT VOD, addressing this issue by utilizing negative activation functions to suppress background noise and eliminating unnecessary long-term dependencies in the temporal sequence.

B. RGBT Object Detection

The incorporation of thermal images alongside RGB images for efficient object detection has become increasingly prevalent. Guan *et al.* [15] initially propose incorporating

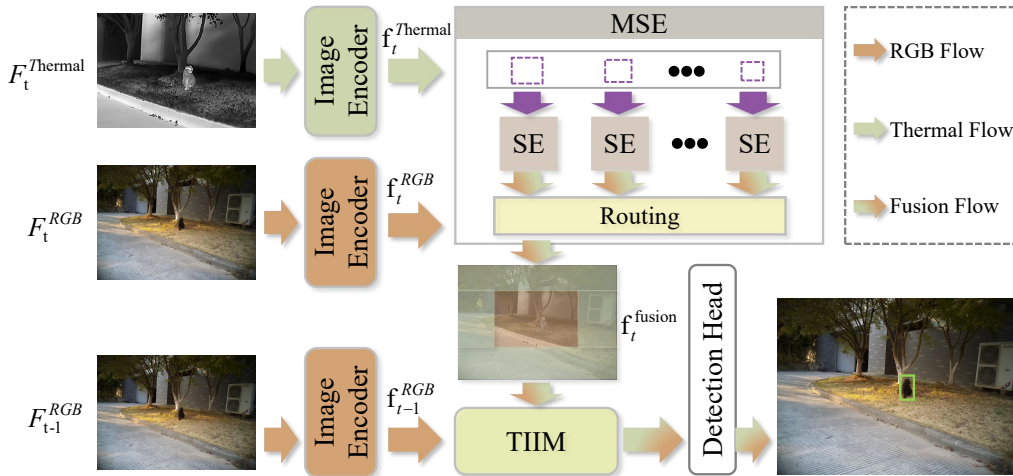


Fig. 2. Architecture diagram of MSENNet. Our objective is to enhance the features of the current frame $Frame_t^{RGB}$; therefore, we do not utilize $Frame_{t-1}^{Thermal}$ for training. This decision is based on the inherent differences in semantics, spatial context, and temporal factors between $Frame_t^{RGB}$ and $Frame_{t-1}^{Thermal}$. Such disparities can negatively affect the fusion effect and reduce operational efficiency.

illumination information into the neural network training process to adaptively adjust the weights of sub-branches, thereby improving the accuracy of pedestrian localization across varied environments. Zhou *et al.* [16] introduce a Modality Balance Network (MBNet) to address the issue of modality imbalance in pedestrian detection. Likewise, generative data augmentation methods are employed for domain adaptation to mitigate modality data imbalances and improve RGBT pedestrian detection performance [17]. Xiang *et al.* [18] propose initially training the feature extractors of both modalities separately, followed by feature fusion across different scales. Zhang *et al.* [19] suggest combining complementary information within and across modalities to jointly capture reliable features, thereby enhancing the foreground features crucial for object detection in each modality. However, these methods all require aligned RGBT image pairs as input, necessitating significant manual effort for data preprocessing.

Zhang *et al.* [20] initial research into pedestrian detection using weakly aligned RGBT images. They introduce a regional feature alignment module to capture positional offsets and facilitate implicit alignment. Subsequently, they extend their work to enhance the prediction method for regional offsets and refine the definition of weak alignment, addressing issues such as object-level offsets and mismatches [3]. Tu *et al.* [21] propose a deep correlation network that utilizes a modality alignment module based on the spatial affine transformation, the feature-wise affine transformation and the dynamic convolution to combine weakly aligned RGBT images for detecting salient objects. However, this weak alignment primarily consists of pixel-level or instance-level adjustments, which still differ from the image-level unaligned data captured by multispectral sensors in real-world scenarios.

III. METHOD

MSENNet is a one-stage video detector that allows for end-to-end training, built upon the YOLOv8 framework [22]. Specifically, YOLOv8 employs the same data loading format

as YOLOv5, which facilitates seamless expansion and integration of multimodal and time-series data into our framework. In contrast, higher versions of YOLO utilize stream-based data loading, which presents challenges in terms of framework scalability and adaptability. Additionally, our empirical evaluations revealed that, in scenarios of the UVT-VOD2024 benchmark, YOLOv8 demonstrates comparable performance and efficiency to higher YOLO (You Only Look Once) counterparts. Given these findings, YOLOv8 emerges as a suitable choice, balancing ease of implementation with robust detection capabilities.

A. Architecture Overview

Fig. 2 illustrates the architecture of the proposed MSENNet. The network is designed to accept three images as input for the training of the current frame, denoted as $Frame_t^{RGB}$. Initially, images from different modalities are processed through their respective encoders to extract features. Importantly, the encoders for different modalities do not share any learnable parameters. Once the features f_t^{RGB} and $f_t^{Thermal}$ are processed, they are input into the MSE, where feature fusion is accomplished through collaborative perception utilizing multiple scale experts. Ultimately, after integrating temporal information, predictions are generated through the detection head.

B. Image Encoder

The image encoder employed in this work is the CSP-DarkNet from the baseline method. This iteration improves upon its predecessor [23] by incorporating an enhanced design that includes additional skip connections and split operations. These architectural refinements not only bolster gradient flow but also significantly enhance the network's overall learning efficacy.

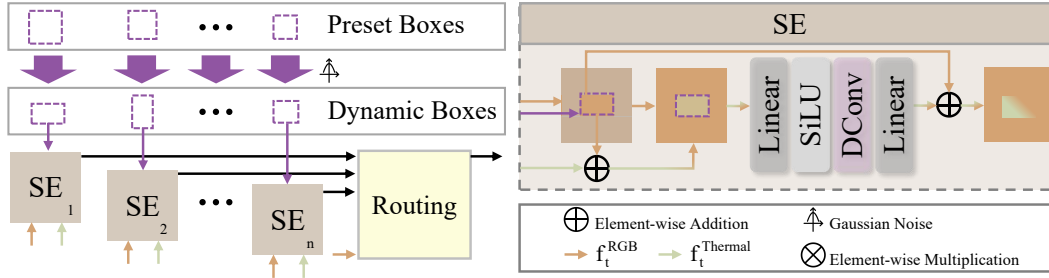


Fig. 3. Flowchart of MSE module. Where “DConv” represents the deformable convolution operation.

C. Mixture of Scale Experts

Prior fusion methodologies often assume the alignment of multi-modal images [24]–[27]. However, RGB and thermal images, which more accurately represent real-world scenarios, frequently exhibit considerable misalignment in scale and spatial distribution. This misalignment necessitates substantial manual effort for processing, and addressing how to circumvent this redundant step in order to enhance the applicability of RGBT VOD in practical situations has emerged as a key challenge.

Our proposed MSE utilizes a set of multi-scale mixture experts to capture the differences between RGBT image pairs at various scales. The detailed structure is illustrated in Fig. 3. We have created a set of anchor boxes of various scales positioned on the f_t^{RGB} , with their dimensions determined by scale factors λ . The sizes of f_t^{RGB} and the predefined anchor box are outlined as follows:

$$\begin{aligned} f_t^{RGB} &= (x, y, w, h) \\ \text{box} &= (x, y, \lambda \times w, \lambda \times h), \end{aligned} \quad (1)$$

where (x, y) denotes the center coordinates, (w, h) represents the width and height. To enhance the network’s robustness against interference, we introduce a small amount of random Gaussian noise to the anchor box size. The quantity of

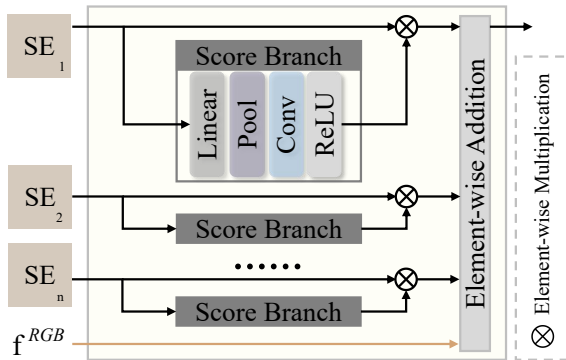


Fig. 4. Flowchart of Routing in MSE.

anchor boxes aligns with the number of scale experts. Each expert employs an anchor box to delineate the corresponding region in f_t^{RGB} , subsequently merging it with the thermal image, thereby accomplishing preliminary alignment of the

two images in spatial scale. For instance-level weak alignment of objects across different modalities, deformable convolution (referred to as DConv in Fig. 3) is utilized to acquire spatial position offsets, facilitating the effective fusion of RGBT. The outcomes from all experts are consolidated through a dynamic routing mechanism.

The schematic diagram of the dynamic routing mechanism is presented in Fig. 4. It takes the outputs of the n experts and the RGB feature map as input. Each expert is associated with a score branch. To prevent bias, the learnable parameters of all score branches are shared. After scoring the fusion results from each expert, the scores are analyzed using the softmax function and employed as weights to dynamically adjust the outputs of all experts. This dynamic routing mechanism enables MSE to adapt different scale distribution discrepancies in RGBT image pairs.

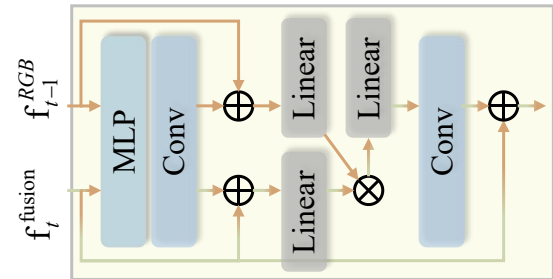


Fig. 5. Flowchart of TIIM.

D. TIIM: Temporal Information Injection Module

In the context of video information processing, we design a Temporal Information Injection Module (TIIM) to efficiently integrate temporal information from neighboring frames into the current frame, a process detailed in Fig. 5. TIIM takes inputs f_t^{fusion} and f_{t-1}^{RGB} and employs a Multi-layer Perceptron (MLP) to converge the feature embedding spaces of the two inputs, followed by a convolutional layer to capture spatial structures. Furthermore, skip connections in both branches ensure the resilience of feature learning. Subsequently, through a linear layer for mapping features, the high-dimensional feature subspace embedding is rapidly accomplished by element-wise multiplication of the feature maps from the two branches.

TABLE I
COMPARISON BETWEEN OUR UVT-VOD2024 AND THE EXISTING DATASET VT-VOD50.

Dataset	Videos	Frames	Categories	Instances	Camera Movement	Scenarios
VT-VOD50	100	18898	7	202847	✗	traffic
UVT-VOD2024 (ours)	174	60988	11	271835	✓	campus, traffic, park countryside, residential zone

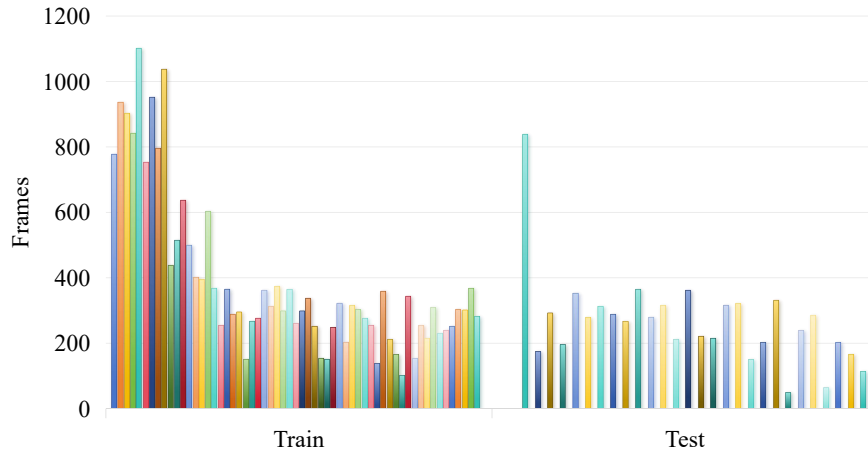


Fig. 6. Training and test sets division of UVT-VOD2024. Each column represents two RGB and Thermal video pairs of exactly the same length, forming a set of multimodal data.

E. Loss Function

MSENet utilizes BCEWithLogitsLoss for computing the classification loss, which integrates both the BCELoss and Sigmoid functions to determine the loss across all category labels. The BCEWithLogitsLoss formula is as follows:

$$L = -[y \cdot \log(\sigma(x)) + (1 - y) \cdot \log(1 - \sigma(x))], \quad (2)$$

where σ denotes the Sigmoid function, x represents the input value, and y signifies the target value, respectively.

For regression loss, the methods employed are Complete Intersection over Union (CIoU) [28] and Distribution Focal Loss (DFL) [29]. CIoU specifically calculates the IOU between the predicted bounding boxes and the ground truth. Ultimately, both the classification loss and regression loss are combined and fed back into the network to contribute to the parameter update process.

IV. UVT-VOD2024: A BENCHMARK FOR ALIGNMENT-FREE RGBT VOD

We have collected a dataset for alignment-free RGBT VOD to assess model performance in this area. In this section, we introduce this dataset, named UVT-VOD2024, in detail.

A. Data Collection and Annotation

The equipment we utilized is the RGBT multi-spectral handheld camera by Hikvision. Data capture spans ten months, encompassing various real-life scenarios. Both modalities record video at 24 frames per second (FPS), with RGB video resolution at 1600×1200 and thermal video resolution at 640×480 . We adopt a dynamic approach to photographing

both moving and stationary objects. Data collection occurs outdoors, encompassing typical settings such as campuses, rural areas, and town roads. Subsequently, we clean data by excluding videos with blurred object definitions and severe shaking. Following this, we annotate and categorize the remaining videos.

We utilize the image annotation tool LabelImg for annotating the dataset. Due to resolution and scale inconsistencies between the two modalities, we adopt the annotation method employed in the RGBT VOD task, which involves annotating each frame of the RGB video with ground truth values. For UVT-VOD2024, we provide annotation formats in VOC [30] and COCO [31], which are compatible with most detection models' input requirements. Ten students dedicate three months to completing the annotation process, with an additional month for verification to ensure consistency across annotations and mitigate potential human-induced errors.

B. Data Description

UVT-VOD2024 represents a significant advancement over the VT-VOD50 [1], in terms of both scale and scenarios. Detailed metrics are provided in Table I. The UVT-VOD2024 dataset comprises 174 videos of varying sizes, totaling 30,494 pairs of RGBT images. Of these, 118 videos are allocated for training the network, while the remaining 56 videos are reserved for evaluating its performance. Fig. 6 illustrates the specific contents of both the training and test sets. Fig. 7 displays two pairs of unaligned raw images captured from our multispectral sensor. Within the UVT-VOD2024, we predefine eleven common categories of daily life scenes, with their names and distributions depicted in Fig. 8. Each category



Fig. 7. Examples of unaligned RGBT image pairs in UVT-VOD2024.

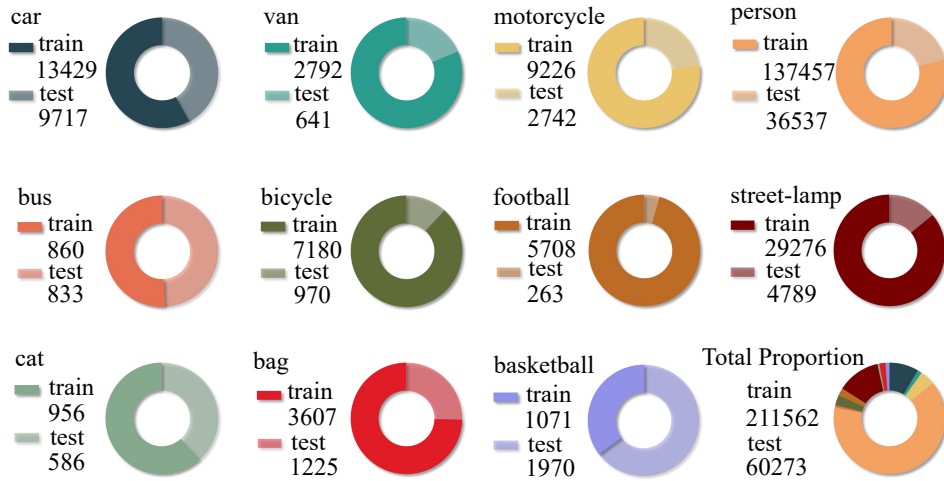


Fig. 8. Details of the category and instance distribution in UVT-VOD2024.

contains a sufficient number of instances to enable comprehensive learning of their characteristics by the network. To more accurately reflect the complexities encountered in real-world applications, we have also introduced challenging cases with imbalanced category distributions. For instance, in the UVT-VOD2024 dataset, the instance distribution of bus is relatively sparse, the number of football instances varies significantly between the training and test sets, and basketball instances are more prevalent in the test set than in the training set. These imbalances highlight the challenges faced by object detection tasks when dealing with limited or unevenly distributed data. On one hand, these challenges effectively assess the model’s performance. On the other hand, they provide a foundation for enhancing model performance, thereby increasing the likelihood of its successful application in real-world scenarios.

UVT-VOD2024 follows the classic VOC dataset format, with benchmarks and evaluation results established based on its standards, as detailed in the experimental section. Free access to UVT-VOD2024 is provided to facilitate public use of the dataset and ensure the reproducibility and accuracy of the research.

V. EXPERIMENTS

In this section, we begin by introducing the experimental setup and foundational parameters. Subsequently, we compare

and analyze our MSENNet against existing methodologies. Following this, we conduct a series of ablation experiments to demonstrate the effectiveness of each component in our design.

A. Datasets and Metrics

In addition to the UVT-VOD2024 dataset introduced in this study, we also assess the model’s performance using the aligned VT-VOD50 dataset [1], which is specifically designed for RGBT VOD. To accommodate algorithms that only process unimodal inputs, we incorporate multi-modal data by performing pixel-wise addition of the RGB and thermal images at the network input.

The evaluation criteria for the model are composed of two primary aspects. The first aspect quantifies the number of parameters and computational load, providing insight into the scale and size of the model. The second aspect evaluates model performance, where Average Precision (AP) serves as an indicator of accuracy, and Frames Per Second (FPS) reflects detection speed. Additionally, we assess parameters and the computational complexity associated with model size, presenting these findings for reference.

TABLE II

WE EVALUATE MSENNet AND THE CURRENT MAINSTREAM DETECTION MODELS SIMULTANEOUSLY ON UVT-VOD2024 AND VT-VOD50, AND WE HIGHLIGHT THE BEST RESULTS IN **BOLD**. THE “-” INDICATES THAT THE MEASUREMENT CONDITIONS ARE NOT MET OR THAT THE RESULT CANNOT BE OBTAINED.

Methods	Backbone	Type	UVT-VOD2024 (unaligned)		VT-VOD50 (aligned)		FPS	Params(M)	FLOPs(G)
			AP50(%)	AP(%)	AP50(%)	AP(%)			
YOLOV3 [32]	Darknet53	Image	25.6	13.5	33.9	17.4	69.9	103.7	283
YOLOV5_M [23]	CSPDarknet53	Image	23.9	12.5	-	-	294.1	25.1	64.4
CFT [33]	CFB	Image	6.7	2.4	42.5	18.9	222.2	73.7	-
YOLOX_L [34]	Darknet53	Image	16.3	-	-	-	104.8	54.2	155.8
YOLOV6_M [35]	EfficientRep	Image	22.7	12.1	-	-	169.5	52	161.6
YOLOV7 [36]	CSPDarknet53	Image	23	10.4	37.7	16.5	294.1	36.5	103.3
YOLOV9-C [37]	GELAN	Image	27.3	14.5	49.1	26.9	99	25.5	103.7
YOLOV10-M [38]	CSPNet	Image	17.1	8.7	46.2	25.2	210	16.5	64
Efficientdet [39]	EfficientNet	Image	20.2	8.8	-	-	87	20.0	100
TOOD [40]	ResNet-50	Image	15.9	7.3	36.3	19	25.8	32	199
Deformable DETR [41]	ResNet-50	Image	7.7	2.9	42.5	23.3	20.7	41.1	197
RT-DETR [42]	ResNet-50	Image	17	7.9	40.2	21.6	-	42.7	130.5
DINO [43]	ResNet-50	Image	29.4	13.7	47.4	25.9	16.7	47.7	274
AlignDETR [44]	ResNet-50	Image	21.1	9.2	-	-	12.9	47.5	235
DDQ DETR [45]	ResNet-50	Image	21.1	9.1	48.3	26.5	13	48.3	275
DiffusionDet [46]	ResNet-50	Image	21.4	9.6	46.9	25.1	-	-	-
DFF [47]	ResNet-50	Video	9.2	3.9	33.5	14.1	40.4	62.1	24.9
FGFA [48]	ResNet-50	Video	16.7	-	35.1	15.8	9	64.5	41
RDN [8]	ResNet-50	Video	16.9	-	40	-	11.3	-	-
SELSA [49]	ResNet-50	Video	12.6	4.6	39.4	17.4	10.5	-	-
MEGA [9]	ResNet-50	Video	15.4	-	27.8	-	16.2	-	-
Temporal ROI Align [50]	ResNet-50	Video	11.1	3.9	38	17	5.1	-	-
CVA-Net [51]	ResNet-50	Video	16.4	6.4	39.7	19.7	6.9	41.6	548.1
STNet [52]	ResNet-50	Video	15.7	6.5	38.4	18.4	5	41.6	752.3
EINet [1]	Darknet53	Video	20.7	-	46.3	24	204.2	11.6	78.2
MSENet (ours)	CSPDarknet53	Video	33.6	18.7	50.3	27.6	131.7	13.22	38.88

B. Implementation Details

The MSENNet is developed using YOLOV8 [22] architecture. The experiment is conducted using Python on the PyTorch framework. The network undergoes training for 100 epochs using two NVIDIA GeForce RTX 3090 GPUs, each with a batch size of 18. The training process employs the SGD optimizer with a learning rate of 0.01 and a momentum factor of 0.9. Default settings exclude data augmentation, utilizing solely the basic tone enhancement technique.

C. Comparative Experiment

We utilize the VT-VOD50 and UVT-VOD2024 datasets to perform a comprehensive evaluation and analysis of our proposed MSENNet, alongside established mainstream detectors. The results are illustrated in Table II, and a detailed analysis follows below.

1) *Results on UVT-VOD2024*: First, we examine the results on the UVT-VOD2024 dataset. In terms of the detection accuracy metric AP50, MSENNet shows a 4.2% improvement over the existing state-of-the-art method, DINO [43]. Additionally, MSENNet achieves a detection speed more than seven times faster than DINO, reaching an impressive 131 FPS. However, in terms of inference speed, MSENNet takes approximately twice as long as the fastest models, YOLOv5_M [23] and YOLOV7 [36]. Despite this, it outperforms both models by an average of 10% in AP50, reaching a value of 33.6.

Furthermore, it is observed that most image-based detectors outperform video-based detectors due to the complexity of object scenes in the UVT-VOD2024 dataset. These intricate

scenes pose significant challenges for several two-stage video detectors, particularly regarding the fusion of region proposals. Additionally, the presence of unaligned features, both temporally and spatially, can disrupt the learning process within the current training framework.

Overall, the MSENNet demonstrate a notable speed advantage in experiments comparing Transformer-based [41], [42], [44], [45] and Faster R-CNN-based [47]–[50] detectors. However, due to the multimodal framework and multi-frame input of the MSENNet, it lags behind in speed compared to the one-stage detectors represented by the YOLO series [23], [34]–[36], [38], but with a significant performance lead.

2) *Results on VT-VOD50*: Our proposed MSENNet is effective not only for unaligned RGBT image pairs but also demonstrates robust performance on the aligned VT-VOD50 dataset. The expert configuration used in this evaluation remains unchanged and is consistent with that utilized for the UVT-VOD2024 dataset.

Among all the compared methods, YOLOv9-C [37] achieves the highest detection accuracy, obtaining an AP50 score of 49.1%. Our MSENNet outperforms YOLOv9-C by 1.2% in accuracy and exceeds its detection speed of 99 FPS. On the VT-VOD50 dataset, Transformer-based detection methods generally perform better. In contrast, image-based detectors outperform most video-based detectors in both accuracy and speed.

Based on the comprehensive results presented in Table II, the model size and computational cost of MSENNet are relatively favorable. While MSENNet outperforms the comparison

method in VT-VOD5, the margin is not as substantial as that observed in UVT-VOD2024. This suggests that existing models experience rapid performance degradation when faced with unaligned data, a challenge mitigated more effectively by MSENNet.

D. Ablation Studies

1) Contributions of MSE and TIIM to Proposed MSENNet:

We conduct a set of ablation experiments to illustrate the development of MSENNet from the baseline, as detailed in Table III. In (a), we present the results of baseline training using RGB images alone.

TABLE III

EXPERIMENTAL RESULTS OF DIFFERENT CONFIGURATIONS IN MSENNet.

Groups	MSE	TIIM	AP50(%)	FPS	FLOPs(G)
(a)			22.0	1111.1	8.2
(b)	✓		31.0	162.8	11.44
(c)		✓	24.0	333.3	35.65
(d)	✓	✓	33.6	131.7	38.88

2) *The Impact of Different Expert Configurations in the MSE Module:* In order to investigate the impact of expert configurations on MSENNet, we conducted a series of experiments, with a selection of representative results presented in Table IV. The findings reveal that the optimal performance is achieved with three groups of experts set at perceptual scales of 0.4, 0.6, and 0.8, respectively. However, increasing the scale factors by 0.1 results in a decline in MSENNet’s detection performance. Furthermore, upon increasing the number of experts to four and five, the network’s performance exhibits slight fluctuations. Notably, the inclusion of experts with smaller scale factors, such as 0.1 and 0.2, generally compromises MSENNet’s performance. This decline can be attributed to the fact that scale differences of 0.1 and 0.2 do not align with the fundamental distribution laws of data in the UVT-VOD2024 dataset.

3) *Assessment of the Structure in MSE:* To demonstrate the effectiveness of Gaussian noise and deformable convolution used in the MSE module, we conduct a set of experiments, with the results shown in Table V. The results demonstrate that incorporating solely the deformable convolutional layer within the MSE module yields a 2.7% enhancement in performance. In contrast, employing only Gaussian noise results in a 1.2% improvement. However, when these two techniques are combined, there is an additional performance boost, thereby validating the efficacy and complementary nature of both approaches.

4) *The Potential of MSE for Scene Generalization:* As previously mentioned, MSENNet retains the identical expert configuration for both UVT-VOD2024 and VT-VO50 in Table II. However, the scale factors ranging from 0.4 to 0.8 are notably more adept at handling unaligned RGBT images. We modify the configuration to endow an expert with a perceptual scale factor of 0.95, as presented in Table VI. The comparison results presented in Table VI are derived from the VT-VOD50

TABLE IV

EXPERIMENTAL RESULTS ON DIFFERENT EXPERT CONFIGURATIONS. WE HIGHLIGHT THE BEST RESULTS IN **BOLD**. HERE, “‡” SYMBOLIZES THE CONFIGURATION EMPLOYED BY OUR PROPOSED METHOD.

Number of Experts	Experts’ Scale	AP50(%)	AP(%)
1	0.3	24.2	12.8
1	0.4	25.5	13.2
1	0.5	25.7	13.0
1	0.6	26.9	13.7
1	0.7	26.3	13.2
1	0.8	30.1	14.5
2	0.6, 0.8	29.3	15.1
2	0.4, 0.6	28.4	14.7
2	0.4, 0.8	32.2	16.9
‡ 3	0.4, 0.6, 0.8	33.6	18.7
3	0.5, 0.7, 0.9	31.2	15.3
4	0.2, 0.4, 0.6, 0.8	29.6	16.2
4	0.3, 0.5, 0.7, 0.9	32.5	17
5	0.2, 0.4, 0.6, 0.8, 0.95	30.3	16.5
5	0.1, 0.3, 0.5, 0.7, 0.95	30.2	15.6

TABLE V

ABLATION STUDY RESULTS OF COMPONENTS IN THE MSE MODULE. THE RESULTS IN THIS TABLE ARE BASED ON MSENNet. WE HIGHLIGHT THE BEST RESULTS IN **BOLD**.

Type	AP50(%)	AP(%)
w/o Score Branch	29.2	15.1
w/o Gaussian Noise	31.9	16.1
w/o Deformable Convolution	30.4	15.3
joint w/ MSE (ours)	33.6	18.7

with aligned RGBT image pairs. Specifically, MSENNet^a denotes the configuration in Table II, which comprises three experts with perception scales set at 0.4, 0.6, and 0.8. In contrast, MSENNet^b builds upon the MSENNet^a configuration by incorporating an additional expert with a perception scale of 0.95. This design choice is motivated by the fact that, objectively, a scale closer to 1 is more appropriate for scenarios involving aligned data.

The results in Table VI confirm our hypothesis that MSENNet achieves higher detection accuracy for aligned RGBT image pairs when incorporating experts with a larger perceptual scale (0.95). Specifically, MSENNet^b improves AP50 by seven percentage points compared to MSENNet^a. To further investigate the impact of different expert configurations on MSENNet’s performance in the aligned data scenario, we conduct additional extensive experiments, the results of which are shown in Table VII.

The results in Table VII demonstrate that in the scenario where RGB and Thermal images are aligned, experts with larger scales in MSENNet consistently outperform those with smaller scales. Interestingly, on aligned data, relying solely on an expert with a larger perceptual scale factor yields satisfactory performance but still falls short of the performance achieved when additional experts with scales of 0.4, 0.6, and 0.8 are included. This finding appears to contradict our initial intuition. Why, then, does a smaller scale factor enhance the performance of MSENNet in the aligned data scenario? Our analysis suggests that although the VT-VOD50 dataset features aligned RGBT image pairs, the entire feature map’s interaction

TABLE VI

COMPARATIVE EXPERIMENTAL RESULTS OF DIFFERENT CONFIGURATIONS OF MSENET ON THE VT-VOD50 DATASET ARE PRESENTED. THE CONFIGURATION OF MSENET^a IS CONSISTENT WITH THAT DESCRIBED IN TABLE II. IN CONTRAST, MSENET^b INCORPORATES AN ADDITIONAL GROUP OF EXPERTS WITH A SCALE OF 0.95. WE HIGHLIGHT THE BEST RESULTS IN **BOLD**.

Methods	AP50(%)	AP(%)
YOLOV3 [32]	33.9	17.4
CFT [33]	42.5	18.9
YOLOV7 [36]	37.7	16.5
YOLOV9-C [37]	49.1	26.9
YOLOV10-M [38]	46.2	25.2
TOOD [40]	36.3	19
Deformable DETR [41]	42.5	23.3
RT-DETR [42]	40.2	21.6
DINO [43]	47.4	25.9
DDQ DETR [45]	48.3	26.5
DiffusionDet [46]	46.9	25.1
DFF [47]	33.5	14.1
FGFA [48]	15.8	9
SELSA [49]	39.4	17.4
MEGA [9]	27.8	-
Temporal ROI Align [50]	38	17
CVA-Net [51]	39.7	19.7
STNet [52]	38.4	18.4
EinNet [1]	46.3	24
MSENet ^a (ours)	50.3	27.6
MSENet ^b (ours)	57.3	31.4

is not always necessary for all images. When the object distribution occupies a small portion of the spatial domain in some images, the network tends to focus on the local regions of the feature map. In such cases, experts with smaller perceptual scale factors play a crucial role.

In summary, the proposed MSENET not only performs well on the unaligned UVT-VOD2024 dataset introduced in this study but also adapts effectively to aligned datasets such as VT-VOD50 by adjusting the configuration of experts. This capability underscores the flexibility and robustness of MSENET.

TABLE VII

THE IMPACT OF DIFFERENT EXPERT CONFIGURATIONS ON THE PERFORMANCE OF MSENET ON THE ALIGNMENT DATASET VT-VOD50. WE HIGHLIGHT THE BEST RESULTS IN **BOLD**.

Number of Experts	Experts' Scale	AP50(%)
4	0.4, 0.6, 0.8, 0.95	57.3
3	0.4, 0.6, 0.8	50.3
2	0.8, 0.95	55.1
2	0.6, 0.95	54.7
1	0.95	54.3
1	0.8	52.4
1	0.6	50.2

E. Robustness of MSENET under Different Alignment Challenges

When we introduce the UVT-VOD2024 dataset, we mention that the data are captured using a handheld Hikvision multi-spectral camera. For this device, the difference in viewing angle between RGB and Thermal images is nearly constant. While minor fluctuations may arise due to camera movement, the overall stability of this difference poses a unique challenge

to the robustness of the network. To thoroughly assess the robustness of MSENET, we design a series of experiments. We construct a spatial transformation function designed to crop and translate the input image spatially. During training, we apply these spatial transformations independently to RGB and Thermal images. This approach enables us to simulate the varying alignments that arise when multimodal image pairs are captured by RGBT cameras with differing parameters. The above process is shown in Fig. 9. We record the results of the experiment in Table VIII.

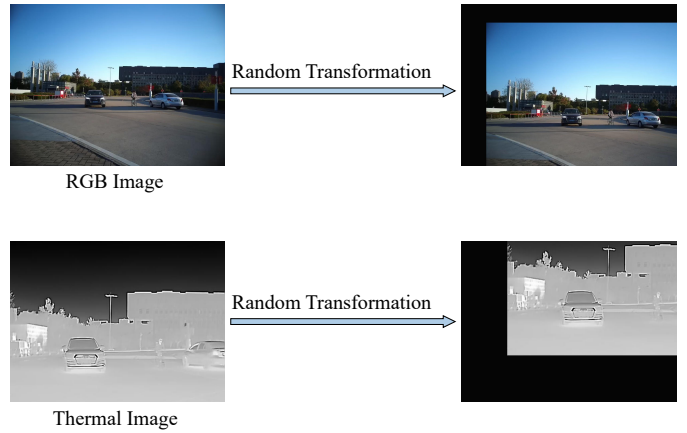


Fig. 9. We employ distinct displacement parameters to conduct random spatial transformations on RGB and Thermal images separately, thereby simulating the varying degrees of spatial misalignment that may arise due to differences in camera configurations.

TABLE VIII

EFFECTS OF DIFFERENT RANGES OF SPATIAL TRANSFORMATIONS ON THE PERFORMANCE OF MSENET FOR RGB AND THERMAL IMAGES. TO FACILITATE A COMPREHENSIVE COMPARISON OF PERFORMANCE DIFFERENCES, WE ADDITIONALLY PRESENT THE PERFORMANCE METRICS OF MSENET WHEN NO SPATIAL TRANSFORMATION IS APPLIED TO THE INPUT IMAGES.

Transformed Image	Offset Pixels	AP50(%)	AP(%)
- (ours)	0	33.6	18.7
RGB	25	22	11
	50	23.8	11.2
	75	21.3	10.6
Thermal	25	31.9	14.7
	50	28	12.7
	75	26.9	12.5

Table VIII demonstrates that spatial transformations of RGB images significantly impact network performance. This phenomenon arises because the training data annotations pertain exclusively to the original RGB images. Consequently, when the spatial configuration of RGB images is altered, ambiguity arises between the transformed images and their annotations, leading to a notable decline in network learning performance. In contrast, the performance degradation of Thermal images under spatial transformations is relatively minor. For instance, when the Thermal image is offset by 25 pixels, the detection accuracy decreases by only 1.7% at an IoU threshold of 50. This resilience is attributed to the inherent characteristics of the UVT-VOD2024 dataset, which features a small thermal

image perspective space that aligns well with the learning principles of MSENNet. However, as the displacement pixel value in spatial transformations increases, the detection accuracy of MSENNet diminishes. This is because the Thermal image provides progressively less supplementary information to the RGB image under larger displacements.

In summary, Table VIII substantiates that MSENNet can achieve robust detection results even in the presence of perspective deviations, which may stem from variations in camera devices.

VI. DISCUSSION AND FUTURE WORK

This paper represents the pioneering effort to liberate RGBT VOD tasks from the limitations of aligned data, achieving notable progress in this domain. However, MSENNet remains reliant on manual expert settings, which necessitate manual adjustments in expert configurations when confronted with significant changes in data scenarios. For instance, transitioning from the unaligned UVT-VOD2024 dataset to the aligned VT-VOD50 dataset requires reconfigurations that limit the model's adaptability and scalability.

These limitations have prompted us to delve deeper into several critical issues. First and foremost is the challenge of achieving RGBT VOD without alignment while eschewing dependence on pre-defined expert settings. This involves developing more autonomous and adaptive mechanisms that can dynamically adjust to varying data characteristics without human intervention. Additionally, we aim to address more extreme scenarios, such as cases where the viewing angle of Thermal images significantly exceeds that of RGB images. These scenarios introduce unique challenges, such as increased misalignment and potential loss of complementary information, which current methods struggle to handle effectively.

In our future work, we will continue to explore these directions with the goal of enhancing the robustness, adaptability, and generalizability of RGBT VOD models.

VII. CONCLUSION

This paper introduces MSENNet, a novel framework designed for alignment-free RGBT VOD to more accurately adapt real-world imaging conditions. MSENNet employs a set of scale-sensitive experts that collectively detect spatial discrepancies between input image pairs and dynamically route to select the most appropriate expert. This mechanism enables the identification of matching regions in RGB images corresponding to Thermal images, thereby achieving coarse alignment. Subsequently, deformable convolution is utilized to address weak alignment issues between objects in RGB and Thermal images. Additionally, we have established the UVT-VOD2024 benchmark dataset for alignment-free RGBT VOD. This dataset encompasses a wide range of life scenes and diverse weather conditions, comprising 60,988 images across 11 common categories with 271,835 object instances.

While MSENNet effectively handles both aligned and unaligned data, its performance partially relies on predefined manual rules. In future work, we aim to develop more resilient

and universal detectors that can operate without such dependencies, thereby enhancing the robustness and adaptability of alignment-free RGBT VOD models.

REFERENCES

- [1] Z. Tu, Q. Wang, H. Wang, K. Wang, and C. Li, "Erasure-based interaction network for rgbt video object detection and a unified benchmark," *arXiv preprint arXiv:2308.01630*, 2023.
- [2] J. Liu, X. Fan, Z. Huang, G. Wu, R. Liu, W. Zhong, and Z. Luo, "Target-aware dual adversarial learning and a multi-scenario modality benchmark to fuse infrared and visible for object detection," in *Proceedings of the IEEE/CVF Conference on Computer Vision and Pattern Recognition*, 2022, pp. 5802–5811.
- [3] L. Zhang, Z. Liu, X. Zhu, Z. Song, X. Yang, Z. Lei, and H. Qiao, "Weakly aligned feature fusion for multimodal object detection," *IEEE Transactions on Neural Networks and Learning Systems*, 2021.
- [4] N. Wanchaitanawong, M. Tanaka, T. Shibata, and M. Okutomi, "Multi-modal pedestrian detection with large misalignment based on modal-wise regression and multi-modal iou," in *2021 17th international conference on machine vision and applications (MVA)*. IEEE, 2021, pp. 1–6.
- [5] M. Yuan, X. Shi, N. Wang, Y. Wang, and X. Wei, "Improving rgb-infrared object detection with cascade alignment-guided transformer," *Information Fusion*, vol. 105, p. 102246, 2024.
- [6] K. Song, X. Xue, H. Wen, Y. Ji, Y. Yan, and Q. Meng, "Misaligned visible-thermal object detection: A drone-based benchmark and baseline," *IEEE Transactions on Intelligent Vehicles*, 2024.
- [7] L. Liu, C. Li, A. Zheng, J. Tang, and Y. Xiang, "Non-aligned rgbt tracking via joint temporal-iterated homography estimation and multi-modal transformer fusion," in *Computer and Information Science and Engineering: Volume 16*. Springer, 2024, pp. 17–32.
- [8] J. Deng, Y. Pan, T. Yao, W. Zhou, H. Li, and T. Mei, "Relation distillation networks for video object detection," in *Proceedings of the IEEE/CVF International Conference on Computer Vision*, 2019, pp. 7023–7032.
- [9] Y. Chen, Y. Cao, H. Hu, and L. Wang, "Memory enhanced global-local aggregation for video object detection," in *Proceedings of the IEEE/CVF Conference on Computer Vision and Pattern Recognition*, 2020, pp. 10 337–10 346.
- [10] L. He, Q. Zhou, X. Li, L. Niu, G. Cheng, X. Li, W. Liu, Y. Tong, L. Ma, and L. Zhang, "End-to-end video object detection with spatial-temporal transformers," in *Proceedings of the 29th ACM International Conference on Multimedia*, 2021, pp. 1507–1516.
- [11] G. Sun, Y. Hua, G. Hu, and N. Robertson, "Efficient one-stage video object detection by exploiting temporal consistency," in *European Conference on Computer Vision*. Springer, 2022, pp. 1–16.
- [12] Y. Shi, N. Wang, and X. Guo, "Yolov: Making still image object detectors great at video object detection," in *Proceedings of the AAAI Conference on Artificial Intelligence*, vol. 37, no. 2, 2023, pp. 2254–2262.
- [13] G. Sun, Y. Hua, G. Hu, and N. Robertson, "Mamba: Multi-level aggregation via memory bank for video object detection," *arXiv preprint arXiv:2401.09923*, 2024.
- [14] S. Moorthy, S. S. KS, S. Arthanari, J. H. Jeong, and Y. H. Joo, "Hybrid multi-attention transformer for robust video object detection," *Engineering Applications of Artificial Intelligence*, vol. 139, p. 109606, 2025.
- [15] D. Guan, Y. Cao, J. Yang, Y. Cao, and M. Y. Yang, "Fusion of multispectral data through illumination-aware deep neural networks for pedestrian detection," *Information Fusion*, vol. 50, pp. 148–157, 2019.
- [16] K. Zhou, L. Chen, and X. Cao, "Improving multispectral pedestrian detection by addressing modality imbalance problems," in *Computer Vision—ECCV 2020: 16th European Conference, Glasgow, UK, August 23–28, 2020, Proceedings, Part XVIII 16*. Springer, 2020, pp. 787–803.
- [17] M. Kieu, L. Berlincioni, L. Galteri, M. Bertini, A. D. Bagdanov, and A. Del Bimbo, "Robust pedestrian detection in thermal imagery using synthesized images," in *2020 25th International Conference on Pattern Recognition (ICPR)*. IEEE, 2021, pp. 8804–8811.
- [18] J. Xiang, S. Gou, R. Li, and Z. Zheng, "Rgb-thermal based pedestrian detection with single-modal augmentation and roi pooling multiscale fusion," in *IGARSS 2022-2022 IEEE International Geoscience and Remote Sensing Symposium*. IEEE, 2022, pp. 3532–3535.

- [19] Y. Zhang, H. Yu, Y. He, X. Wang, and W. Yang, "Illumination-guided rgbt object detection with inter-and intra-modality fusion," *IEEE Transactions on Instrumentation and Measurement*, vol. 72, pp. 1–13, 2023.
- [20] L. Zhang, X. Zhu, X. Chen, X. Yang, Z. Lei, and Z. Liu, "Weakly aligned cross-modal learning for multispectral pedestrian detection," in *Proceedings of the IEEE/CVF International Conference on Computer Vision*, 2019, pp. 5127–5137.
- [21] Z. Tu, Z. Li, C. Li, and J. Tang, "Weakly alignment-free rgbt salient object detection with deep correlation network," *IEEE Transactions on Image Processing*, vol. 31, pp. 3752–3764, 2022.
- [22] G. Jocher, A. Chaurasia, and J. Qiu, "Ultralytics YOLO," Jan. 2023. [Online]. Available: <https://github.com/ultralytics/ultralytics>
- [23] G. Jocher, "Ultralytics yolov5," 2020. [Online]. Available: <https://github.com/ultralytics/yolov5>
- [24] L. Zhang, Z. Liu, X. Chen, and X. Yang, "The cross-modality disparity problem in multispectral pedestrian detection," *arXiv preprint arXiv:1901.02645*, 2019.
- [25] H. Zhang, E. Fromont, S. Lefèvre, and B. Avignon, "Guided attentive feature fusion for multispectral pedestrian detection," in *Proceedings of the IEEE/CVF winter conference on applications of computer vision*, 2021, pp. 72–80.
- [26] L. Tang, J. Yuan, H. Zhang, X. Jiang, and J. Ma, "Piafusion: A progressive infrared and visible image fusion network based on illumination aware," *Information Fusion*, vol. 83, pp. 79–92, 2022.
- [27] R. Li, J. Xiang, F. Sun, Y. Yuan, L. Yuan, and S. Gou, "Multiscale cross-modal homogeneity enhancement and confidence-aware fusion for multispectral pedestrian detection," *IEEE Transactions on Multimedia*, vol. 26, pp. 852–863, 2023.
- [28] Z. Zheng, P. Wang, D. Ren, W. Liu, R. Ye, Q. Hu, and W. Zuo, "Enhancing geometric factors in model learning and inference for object detection and instance segmentation," *IEEE transactions on cybernetics*, vol. 52, no. 8, pp. 8574–8586, 2021.
- [29] X. Li, C. Lv, W. Wang, G. Li, L. Yang, and J. Yang, "Generalized focal loss: Towards efficient representation learning for dense object detection," *IEEE Transactions on Pattern Analysis and Machine Intelligence*, vol. 45, no. 3, pp. 3139–3153, 2023.
- [30] M. Everingham, L. Van Gool, C. K. I. Williams, J. Winn, and A. Zisserman, "The pascal visual object classes (voc) challenge," *International Journal of Computer Vision*, vol. 88, no. 2, pp. 303–338, Jun. 2010.
- [31] T.-Y. Lin, M. Maire, S. Belongie, J. Hays, P. Perona, D. Ramanan, P. Dollár, and C. L. Zitnick, "Microsoft coco: Common objects in context," in *Computer Vision—ECCV 2014: 13th European Conference, Zurich, Switzerland, September 6–12, 2014, Proceedings, Part V 13*. Springer, 2014, pp. 740–755.
- [32] J. Redmon and A. Farhadi, "Yolov3: An incremental improvement," *arXiv preprint arXiv:1804.02767*, 2018.
- [33] F. Qingyun, H. Dapeng, and W. Zhaokui, "Cross-modality fusion transformer for multispectral object detection," *arXiv preprint arXiv:2111.00273*, 2021.
- [34] Z. Ge, S. Liu, F. Wang, Z. Li, and J. Sun, "Yolox: Exceeding yolo series in 2021," *arXiv preprint arXiv:2107.08430*, 2021.
- [35] C. Li, L. Li, H. Jiang, K. Weng, Y. Geng, L. Li, Z. Ke, Q. Li, M. Cheng, W. Nie *et al.*, "Yolov6: A single-stage object detection framework for industrial applications," *arXiv preprint arXiv:2209.02976*, 2022.
- [36] C.-Y. Wang, A. Bochkovskiy, and H.-Y. M. Liao, "Yolov7: Trainable bag-of-freebies sets new state-of-the-art for real-time object detectors," in *2023 IEEE/CVF Conference on Computer Vision and Pattern Recognition (CVPR)*, 2023, pp. 7464–7475.
- [37] C.-Y. Wang, I.-H. Yeh, and H.-Y. M. Liao, "Yolov9: Learning what you want to learn using programmable gradient information," *arXiv preprint arXiv:2402.13616*, 2024.
- [38] A. Wang, H. Chen, L. Liu, K. Chen, Z. Lin, J. Han, and G. Ding, "Yolov10: Real-time end-to-end object detection," *arXiv preprint arXiv:2405.14458*, 2024.
- [39] M. Tan, R. Pang, and Q. V. Le, "Efficientdet: Scalable and efficient object detection," in *Proceedings of the IEEE/CVF Conference on Computer Vision and Pattern Recognition*, 2020, pp. 10 781–10 790.
- [40] C. Feng, Y. Zhong, Y. Gao, M. R. Scott, and W. Huang, "Tood: Task-aligned one-stage object detection," in *2021 IEEE/CVF International Conference on Computer Vision (ICCV)*. IEEE Computer Society, 2021, pp. 3490–3499.
- [41] X. Zhu, W. Su, L. Lu, B. Li, X. Wang, and J. Dai, "Deformable detr: Deformable transformers for end-to-end object detection," in *International Conference on Learning Representations*, 2021. [Online]. Available: <https://openreview.net/forum?id=gZ9hCDWe6ke>
- [42] Y. Zhao, W. Lv, S. Xu, J. Wei, G. Wang, Q. Dang, Y. Liu, and J. Chen, "Detrs beat yolos on real-time object detection," in *Proceedings of the IEEE/CVF Conference on Computer Vision and Pattern Recognition*, 2024, pp. 16 965–16 974.
- [43] H. Zhang, F. Li, S. Liu, L. Zhang, H. Su, J. Zhu, L. M. Ni, and H.-Y. Shum, "Dino: Detr with improved denoising anchor boxes for end-to-end object detection," *arXiv preprint arXiv:2203.03605*, 2022.
- [44] Z. Cai, S. Liu, G. Wang, Z. Ge, X. Zhang, and D. Huang, "Align-detr: Improving detr with simple iou-aware bce loss," *arXiv preprint arXiv:2304.07527*, 2023.
- [45] S. Zhang, X. Wang, J. Wang, J. Pang, C. Lyu, W. Zhang, P. Luo, and K. Chen, "Dense distinct query for end-to-end object detection," in *Proceedings of the IEEE/CVF Conference on Computer Vision and Pattern Recognition*, 2023, pp. 7329–7338.
- [46] S. Chen, P. Sun, Y. Song, and P. Luo, "Diffusiondet: Diffusion model for object detection," in *Proceedings of the IEEE/CVF International Conference on Computer Vision*, 2023, pp. 19 830–19 843.
- [47] X. Zhu, Y. Xiong, J. Dai, L. Yuan, and Y. Wei, "Deep feature flow for video recognition," in *Proceedings of the IEEE Conference on Computer Vision and Pattern Recognition*, 2017, pp. 2349–2358.
- [48] X. Zhu, Y. Wang, J. Dai, L. Yuan, and Y. Wei, "Flow-guided feature aggregation for video object detection," in *Proceedings of the IEEE International Conference on Computer Vision*, 2017, pp. 408–417.
- [49] H. Wu, Y. Chen, N. Wang, and Z. Zhang, "Sequence level semantics aggregation for video object detection," in *Proceedings of the IEEE/CVF International Conference on Computer Vision*, 2019, pp. 9217–9225.
- [50] T. Gong, K. Chen, X. Wang, Q. Chu, F. Zhu, D. Lin, N. Yu, and H. Feng, "Temporal roi align for video object recognition," in *Proceedings of the AAAI Conference on Artificial Intelligence*, vol. 35, no. 2, 2021, pp. 1442–1450.
- [51] Z. Lin, J. Lin, L. Zhu, H. Fu, J. Qin, and L. Wang, "A new dataset and a baseline model for breast lesion detection in ultrasound videos," in *Medical Image Computing and Computer Assisted Intervention – MICCAI 2022*. L. Wang, Q. Dou, P. T. Fletcher, S. Speidel, and S. Li, Eds. Cham: Springer Nature Switzerland, 2022, pp. 614–623.
- [52] C. Qin, J. Cao, H. Fu, R. M. Anwer, and F. S. Khan, "A spatial-temporal deformable attention based framework for breast lesion detection in videos," in *International Conference on Medical Image Computing and Computer-Assisted Intervention*. Springer, 2023, pp. 479–488.